npj | science of food

Article

Published in partnership with Beijing Technology and Business University & International Union of Food Science and Technology

https://doi.org/10.1038/s41538-025-00639-w

Evolution of the structure and rheology of processed seaweed *Ulva* spp. during in vitro digestion

Antonio Souto-Prieto[1,2] ✉, Angel Cobos[1], Tania Ferreiro[2], Zuriel Castillo[1,2], Laura Díaz-Piñero[3,4], Marta Martínez-Sanz[3,4] & Patricia Lopez-Sanchez[5] ✉

Seaweed is a sustainable and nutrient-rich food source, but its complex cell wall architecture can physically shield its components from digestion, potentially limiting their release and utilisation. This study investigated how mechanical (blending) and thermal (40–100 °C) processing affect the structure, rheology, and digestive behaviour of *Ulva* spp. dispersions. Processing modulated particle size, softness, and polysaccharide solubilisation, influencing the viscosity and viscoelastic properties of the dispersions. During in vitro digestion, gastric viscosity increased over time for all samples, driven by particle swelling, while intestinal viscosity was lower and stable, except in the 100 °C-treated sample, where it increased, suggesting greater release of soluble components. Small-angle X-ray scattering (SAXS) indicated larger nanostructural disruption of the cell wall and release of cell wall components, potentially ulvan, in the 100 °C-treated sample, which might lead to enhanced digestibility. Large unheated particles ($D_{[3,\ 2]}$ ≈100 μm) showed limited breakdown, whereas thermally treated particles exhibited greater degradation during simulated digestion. These findings demonstrate that processing governs both physical structure and digestive performance, enabling the design of seaweed-based foods with improved functionality.

In recent years, seaweeds have gained increasing attention in food science, primarily due to their potential as a sustainable food source with beneficial environmental implications. They can be classified into three types based on their pigments: brown (*Phaeophyceae*), red (*Rhodophyta*), and green (*Chlorophyta*). Currently, the largest production comes from red and brown seaweeds[1], due to their content of hydrocolloids of industrial interest. However, green seaweeds, such as *Ulva* spp., are present worldwide, are eaten fresh in salads or boiled in soups and stews[1] and stand out for their ease of cultivation and favourable nutritional profile, particularly their high protein content (up to 30% dry weight)[2], including essential amino acids comparable to those found in terrestrial plant proteins. For this reason, methods for obtaining *Ulva* protein extracts are being developed as a potential protein source for human consumption[1,3–5]. Furthermore, *Ulva* spp. contain significant amounts of polysaccharides (9–65% dry weight)[1,4,6], such as soluble ulvan. This polysaccharide has demonstrated potential prebiotic effects that support gut health in animal studies[7,8], and in vitro research has also reported its potential anticoagulant, antibacterial, antiviral, and immunoregulatory activities[8].

The digestibility of *Ulva* spp. has been the focus of several studies, particularly in relation to protein digestibility, which is very low in whole raw seaweed, in comparison to other protein sources[1,9,10]. Previous research on the in vitro digestibility of different seaweed species[11] showed that *Ulva rigida* had the lowest protein digestibility. This low protein digestibility has been explained in relation to the large particle size[11] and to the thickness, rigidity[1,11,12] and high content of cell wall polysaccharides in this green seaweed, which can reduce the accessibility and action of digestive enzymes[1,11,12]. Other factors influencing protein digestibility are the interactions between proteins and polysaccharides[9,13]; and the presence of other components in the seaweed, such as trypsin inhibitors, amylase inhibitors, tannins and phytic acid[1,14,15]. Studies have indicated that the biomass digestibility of *Ulva* spp., when it is added to animal feed, depends on several factors, such as

[1]Department of Analytical Chemistry, Nutrition and Food Science, Facultad de Ciencias, Universidade de Santiago de Compostela, Campus Terra, Lugo, 27002, Spain. [2]Dairy Products and Food Technology Center APLTA, Universidade of Santiago de Compostela, Rúa Montirón, Lugo, 27002, Spain. [3]Escuela de doctorado, Universidad Autónoma de Madrid, Francisco Tomas y Valiente 7, Madrid, 28049, Spain. [4]Instituto de Investigación en Ciencias de la Alimentación, CIAL, (CSIC-UAM, CEI UAM + CSIC), Nicolás Cabrera, Madrid, 28049, Spain. [5]Department of Food Technology, Marine Research Institute IIM-CSIC, Rúa de Eduardo Cabello, Vigo, 36208, Spain. ✉e-mail: antonio.s.prieto@usc.es; plopez@iim.csic.es

the inclusion level and the biomass treatment, but in general, the digestibility is low and only increases when protein is supplied as an extract[3,16]. Those studies suggest that the cell wall of *Ulva* spp., with a high fibre content, especially of the polysaccharide ulvan, is indigestible to monogastric animals and can hinder the bioavailability of nutrients if not properly processed[16,17]. Therefore, more research is necessary to fully understand the changes in *Ulva* spp. cell wall structure during human digestion.

Food processing modifies not only the particle size and rheological properties of food but also its digestibility. Smaller particles offer greater surface area for enzymatic action, while larger particles may slow digestion. Viscosity is another critical factor; higher viscosities can reduce enzyme efficiency and delay gastric emptying. This is especially relevant for fibre-rich foods, such as *Ulva* spp., as soluble fibres can increase the viscosity of the digestive fluids, potentially slowing nutrient diffusion and absorption. While moderate viscosity may help modulate digestion, high viscosity could hinder nutrient bioavailability.

The critical viscosity threshold at which food viscosity begins to significantly impede nutrient bioavailability is not uniformly established, as it depends on factors such as nutrient type, food matrix, and digestive conditions. Nevertheless, recent studies provide useful reference points. For instance, in β-carotene nanoemulsions with oatmeal, high viscosities above 250 mPa s were found to reduce fat digestibility and nutrient absorption[18]. Computer simulations modelling starch and glucose digestion indicated that nutrient absorption starts to become limited at around 100 mPa s[19]. In human MRI studies, meals containing dextrose, lipids, and carbohydrates with viscosities of 60 mPa s were sufficiently low to allow rapid mixing and gastric emptying, whereas meals with much higher viscosities of 29,500 mPa s were very thick, slowed gastric emptying, and likely restricted nutrient absorption[20].

Mechanical and thermal processing of red seaweeds has been shown to permeabilise and disrupt cell walls, enhancing protein digestibility, although the effects can vary depending on the seaweed species[13]. Methods used to produce protein concentrates (acid hydrolysis, microwave digestion, alkaline solubilisation and acidic precipitation) also improve in vitro protein digestibility in red seaweeds[21]. For brown seaweed, it has been reported that food processing (high-pressure homogenisation and heat treatment) can influence the micro- and nanostructure of cell walls[22,23], fermentation increases the digestibility of the seaweeds[24,25] and ultrasound treatment of the seaweeds can also increase the digestibility of their proteins[26]. However, studies on the effects of processing conditions on the cell wall structure and digestibility of *Ulva* spp. are limited, with most existing research focusing on isolated protein extracts rather than whole biomass.

Despite significant advancements, several gaps remain in the research on green algae *Ulva* spp. as a food source; in particular, the relationship between processing and digestibility requires further investigation. The aim of this work is to study the effect of blending and thermal treatments on aqueous dispersions of the green seaweed *Ulva* spp., focusing on particle size distribution, microstructure, cell wall nanostructure and rheological properties. Additionally, structural and rheological changes taking place during digestion were assessed using the standardised in vitro INFOGEST protocol. Unlike many previous studies that have emphasised compositional aspects, our work specifically addresses structural and rheological features. The findings of this research can contribute to improving the exploitation of whole green algae in human nutrition.

Table 1 | Chemical composition of *Ulva* spp. Protein, fat, carbohydrates, total fibre and ash are expressed in % of dry matter

Chemical composition	
Protein[a]	20.3 ± 0.20
Fat	3.8 ± 0.3
Carbohydrates	59.8 ± 0.0
Total Fibre	31.5 ± 1.4
Ash	16.1 ± 0.01
Monosaccharides composition (% of total monosaccharides)	
Gal	5.53 ± 3.5
Glu	17.0 ± 0.0
Xyl	2.37 ± 0.66
Rham	36.3 ± 0.74
GlcA	21.1 ± 10.6
IdoA	17.7 ± 10.0

Monosaccharide composition is presented as the relative composition of total monosaccharides (%). *Gal* galactose, *Glu* glucose, *Xyl* xylose, *Rham* rhamnose, *GlcA* glucuronic acid, *IdoA* iduronic acid. Mean ± standard deviation ($n = 3$).
[a]Protein values were calculated with a 5.13 conversion factor.

Results

Chemical composition of *Ulva* spp

The dry matter of the seaweed was 11.4 ± 0.7% (fresh weight), indicating a water content of ca. 89%. The main component was carbohydrates, accounting for 59.8% (dry weight), the total fibre content was 31.5% (dry weight), thus non-fibre carbohydrates accounted for 28.3% (dry weight) (Table 1). The protein content was 20.3% (dry weight), the ash content was 16.1% (dry weight), and the fat content was 3.8% (dry weight). The overall composition agrees well with the previously reported composition of *Ulva* spp.[27]. The main monosaccharides detected were Rham (36.6%), GlucA (21%), IdoA (17.7%), Gluc (17%), Gal (5.5%) and Xyl (2.4%). Rhamnose, xylose, glucuronic acid and iduronic acid are attributed to ulvan[28], a complex sulphated polysaccharide present in the cell wall of green algae. Glucose is related to cellulose, which in green algae could be 15–30% of the total carbohydrates[29,30]. Similar monosaccharide content has been previously reported for *Ulva* spp.[5].

Design of *Ulva* spp. dispersions with controlled particle size and morphology

Aqueous dispersions of *Ulva* spp. prepared by mechanical treatment (blending) showed a bimodal particle size distribution (Fig. 1A), with a large band at ca. 100–1000 μm and a smaller band at ca. 10–100 μm. As the blending time increased, there was a shift toward smaller particle sizes for both bands. The average particle size $D_{[3,2]}$ was reduced with the duration of the treatment (Fig. 1B), going from 145 ± 10 μm at 30 s, 96 ± 3 μm at 60 s, 65 ± 2 μm at 90 s and 56.9 ± 0.3 μm at 120 s. As the reduction in particle size beyond 90 s was smaller, compared to shorter treatment times, a mechanical treatment duration of 90 s was selected for subsequent thermal processing of the dispersions, since shorter processing times are preferred for environmental and economic reasons.

Figure 1C shows the particle size distribution of thermally treated samples. As it can be observed the temperature had a minor effect on the average particle size $D_{[3,2]}$ (Fig. 1D). The largest band observed is likely associated with clusters of cells, while the smallest band may correspond to single cells or cell fragments, as visualised in the micrographs (Fig. 2A, B). Microscopy images further revealed that cell clusters had intact cells, containing intracellular material, and empty cells (Fig. 2C). Moreover, even after a thermal treatment at 100 °C, single cells still retained internal content, as indicated by the green to brownish coloration in the images (Fig. 2D). This coloration is attributed to the presence of chlorophyll and chlorophyll-related metabolites. Similar structures were observed in the dispersions processed at lower temperatures (Supplementary Fig. S1). Thermal treatments can alter cell wall porosity and compromise membrane integrity, thereby influencing digestion; polysaccharide solubilisation reduces wall density, while membrane denaturation above 60 °C enables leakage of cell contents. The pH of all dispersions was between 6.2 and 6.9, and the ζ potential was negative, with values between −15 and −19 mV (Fig. 1D). The ζ potential of the dispersions was similar regardless of the processing

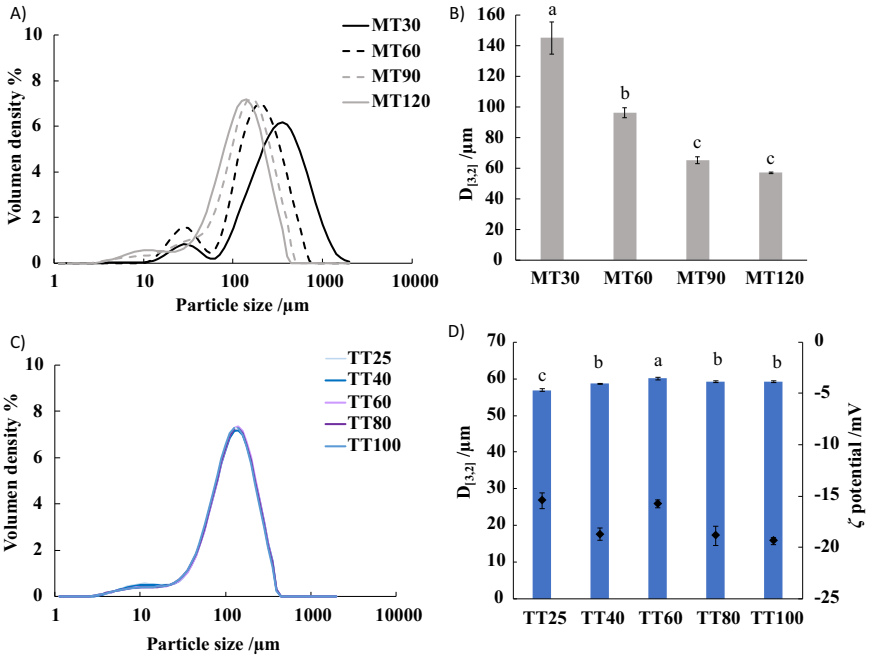

Fig. 1 | Processing conditions determine particle size distribution. A Particle size distribution of *Ulva* spp. dispersions prepared by mechanical treatment for 30 s (MT30), 60 s (MT60), 90 s (MT90) and 120 s (MT120). **B** Average particle size diameter $D_{[3,2]}$ for the same mechanically treated samples. **C** Particle size distribution of *Ulva* spp. dispersions prepared by mechanical treatment for 90 s at 25 °C (TT25), and prepared by mechanical treatment for 90 s followed by thermal treatment for 30 min at 40 °C (TT40), 60 °C (TT60), 80 °C (TT80) and 100 °C (TT100). **D** Average particle size diameter for the same thermally treated samples. The total electrical charge of the samples (ζ potential) is also represented (black diamond symbols in (**D**)). Values in figures with different letters (a, b, c) are significantly different.

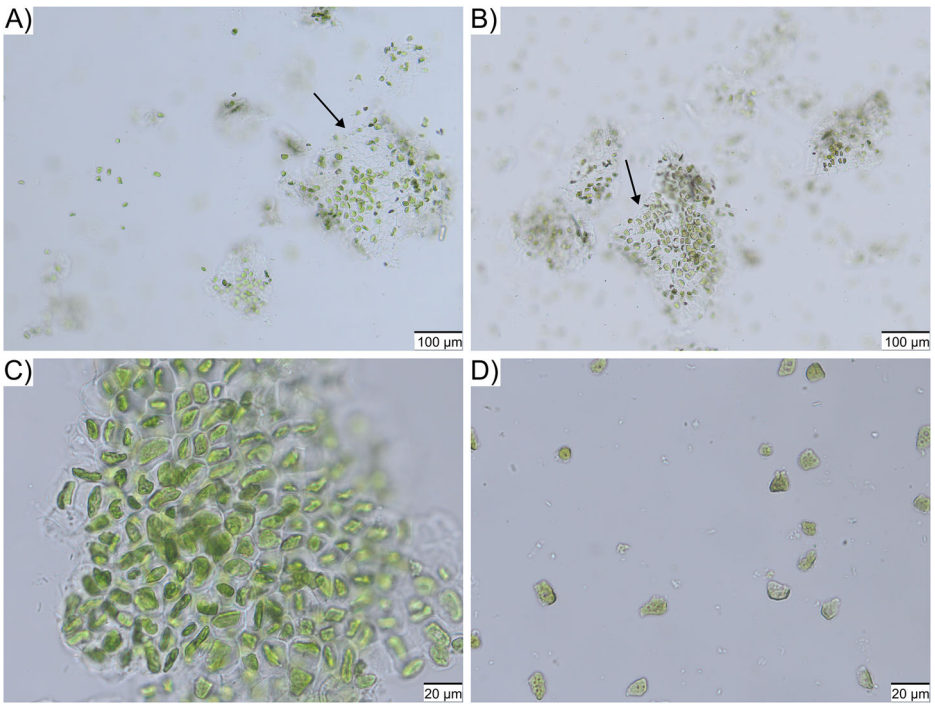

Fig. 2 | Particle morphologies in the dispersions. Micrographs of *Ulva* spp. dispersions showing particle morphology of samples processed by mechanical treatment for 90 s at 25 °C (TT25) (**A**, **C**) and samples processed by mechanical treatment for 90 s followed by thermal treatment for 30 min at 100 °C (TT100) (**B**, **D**). Intracellular content was present after both treatments, as indicated by black arrows. Details of clusters in TT25 (**C**) and single cells in TT100 (**D**).

temperature. These values could indicate moderate stability of the dispersions by electrostatic repulsion, but aggregation and sedimentation could still occur over time.

Nanostructural changes in *Ulva* cell walls induced by processing

To better understand the effects of heating, we used small-angle X-ray scattering (SAXS) to examine the nanostructure of seaweed cell walls in the dispersed phase and the soluble polymers present in the liquid phase of the dispersions. The obtained scattering patterns were represented in Kratky plots to better visualise scattering features. Regarding the dispersed (insoluble) phase (Fig. 3A), all samples showed pronounced scattering features in the low to mid q range (0.01–0.2 $Å^{-1}$). In particular, a small sharp peak was observed at 0.14 $Å^{-1}$, corresponding to a real distance of 4.5 nm, which can be attributed to the interfibrillar distance between tightly packed cellulose microfibrils, similarly to what has been previously reported in plant cell walls[31,32]. This peak was present in all samples, indicating thermal stability of the cellulose microfibrils; however, the intensity of the peak increased slightly in the samples treated at temperatures above 80 °C. This could be explained by water losses, or solubilisation of cell wall components, which led to a greater densification of the cell wall structure, i.e. a greater proportion of cellulose microfibrils were closer to each other. Furthermore, a shoulder-like feature was visible in all the samples.

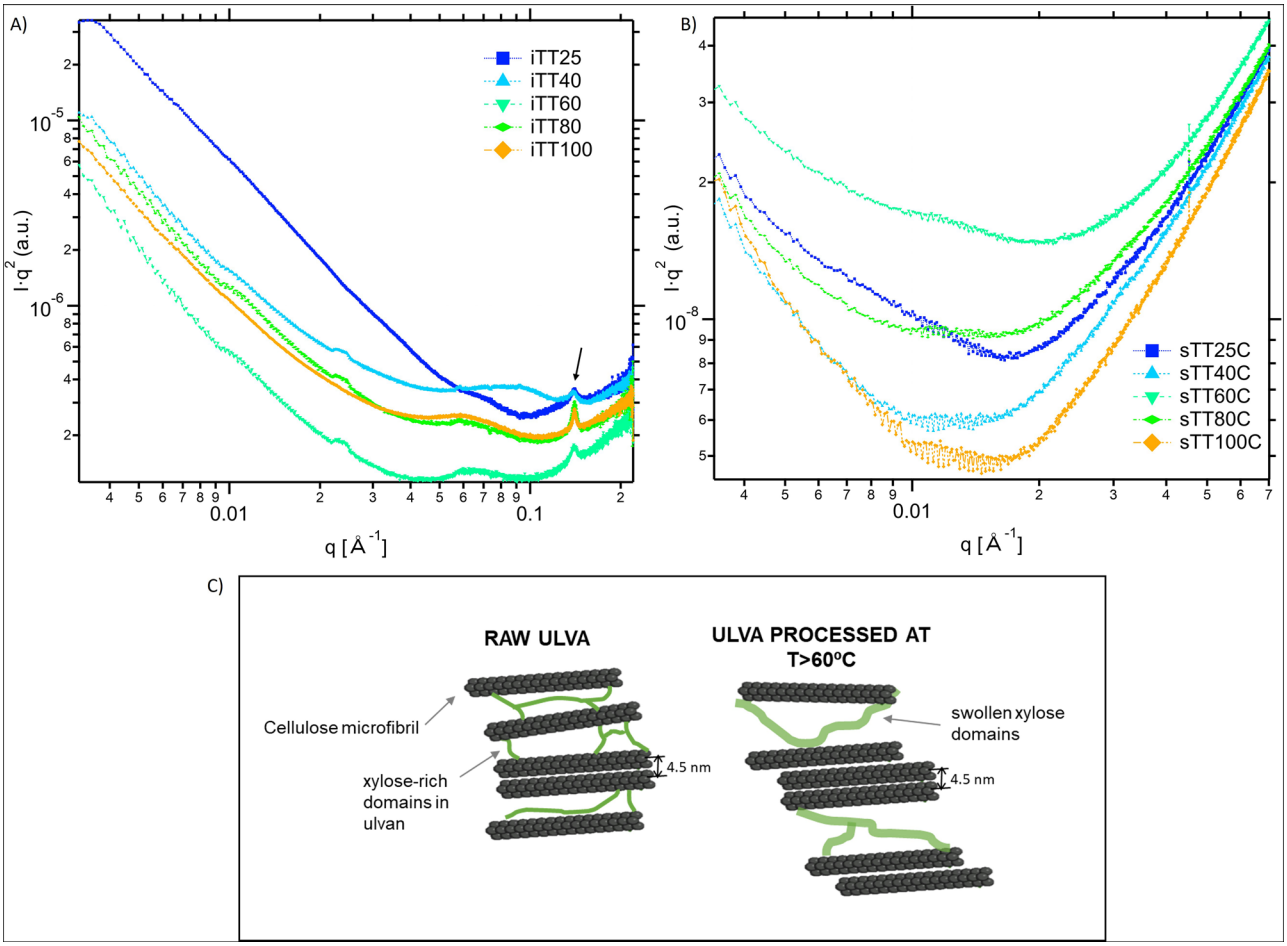

Fig. 3 | Small angle X-ray scattering (SAXS) reveals differences in the nanostructure of the insoluble and soluble fractionof the dispersions. (**A**) SAXS Kratky plots of dispersed phase containing insoluble particles (iTT25, iTT40, iTT60, iTT80 and iTT100) and (**B**) liquid phase (sTT25, sTT40, sTT60, sTT80 and sTT100) of *Ulva* dispersions prepared by mechanical treatment (25 °C) for 90 s followed by thermal treatment during 30 min at 40 °C (TT40), 60 °C (TT60), 80 °C (TT80) and 100 °C (TT100). Dispersed and liquid phases were separated by centrifugation. The black arrow points toward the interfibrillar cellulose peak. (**C**) Squematic representation of the proposed cell wall structure for raw *Ulva* spp. and *Ulva* spp. processed at temperatures above 60 °C. Figures were created using the IRENA macro suite [28] within the Igor software package (Wavemetrics, Lake Oswego, Oregon).

A similar feature has been previously reported in the SAXS patterns from cellulose hydrogels synthesised in the presence of plant cell wall polysaccharides such as xyloglucans[33], and was attributed to cellulose-xyloglucan interactions leading to increased interfibrillar distances in some regions along the cellulose microfibrils. In the case of *Ulva* spp., this shoulder might be indicative of interactions between cellulose and the xylose from ulvans[34]. This shoulder was centred at ca. 0.07 $Å^{-1}$ in the unheated sample (TT25), corresponding to a distance of ca. 9 nm, but the position shifted in the thermally treated samples. We hypothesised that the weak scattering feature detected at ca. 0.01 $Å^{-1}$ (corresponding to a size range ca. 60–65 nm) in the samples treated at 40, 60 and 80 °C could reflect the presence of aggregates, or phase-separated domains, within the polysaccharide matrix of the cell wall. Such structures were not present at 100 °C, perhaps due to degradation at that temperature. Nevertheless, further studies are required to confirm this structural interpretation.

In the liquid (soluble) phase, the SAXS patterns presented a shoulder at $q \approx 0.012$ $Å^{-1}$ (Fig. 3B), corresponding to a real distance of ca. 50 nm, indicating the presence of mesoscale structures in the soluble phase of the *Ulva* dispersions. This shoulder became more pronounced after thermal treatment, likely due to the partial solubilisation of matrix polysaccharides, such as ulvan, although their concentration in the liquid phase remained very low. Ulvan extraction using hot water has been reported[35] yielding extracts with molecular weights in the hundreds of kDa. A measured hydrodynamic diameter of approximately 50 nm, determined by SAXS, may correspond to a molecular weight in the range of 200–1000 kDa or higher, depending on the ulvan chain conformation in solution and the ionic strength. Thus, thermal treatment promoted partial cell wall disassembly and extraction of wall polysaccharides, generating supramolecular assemblies detectable in the SAXS patterns.

Flow behaviour and viscoelastic properties of *Ulva* spp. dispersions

Figure 4A depicts the shear viscosity curves of thermally treated *Ulva* spp. aqueous dispersions (3 wt%). The dispersions were shear thinning, i.e. the viscosity decreased with shear rate. Up to 60 °C, heating did not impact the viscosity of the dispersions, whilst at 80 °C, a significant decrease was observed. At 100 °C, the viscosity was similar to that at 80 °C. The consistency coefficient and flow behaviour index, obtained from power law fitting of the shear stress versus shear rate data, are presented in Table 2.

The non-thermally treated sample (TT25) exhibited a consistency coefficient of 0.8 Pa s^{-n} and a flow behaviour index of 0.5, indicating shear thinning behaviour. The consistency remained similar up to 60 °C and decreased to 0.2 Pa s^{-n} at 80 °C and 100 °C. Simultaneously, the flow behaviour index increased from 0.5 at 25 °C to 0.7 at 100 °C, indicating a shift toward more Newtonian-like behaviour ($n = 1$). The rheology of a dispersion is influenced by both the viscosity of the continuous liquid phase and the volume fraction of the dispersed phase. Therefore, to understand the

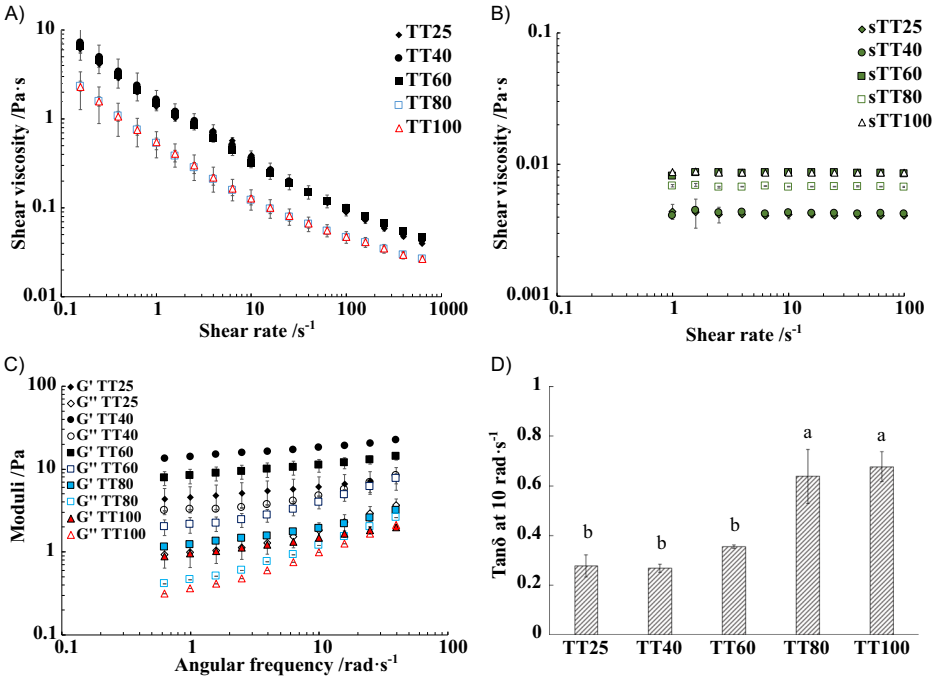

Fig. 4 | Rheological properties of the dispersions. **A** Shear viscosity curves of thermally treated *Ulva* spp. dispersions (3 wt%). **B** Shear viscosity of the corresponding liquid phase containing soluble solids (sTT25, sTT40, sTT60, sTT80 and sTT100) obtained after centrifugation. **C** Storage modulus (G') and loss modulus (G'') as a function of the angular frequency. **D** Average tanδ at 10 rad s^{-1} of thermally treated *Ulva* spp. dispersions 3 wt%. Dispersions were first mechanically treated for 90s (TT25) followed by thermal treatment for 30 min at 40 °C (TT40), 60 °C (TT60), 80 °C (TT80) and 100 °C (TT100). Values in figures with different letters (a, b) are significantly different.

Table 2 | Parameters obtained from the power law fitting (R^2 = 0.99) of the shear stress vs. shear rate data of *Ulva* spp. dispersions

	Consistency coefficient (Pa s^{-n})	Flow behaviour (–)
TT25	1.28 ± 0.76^{a}	0.50 ± 0.06^{b}
TT40	0.82 ± 0.24^{ab}	0.55 ± 0.03^{b}
TT60	0.68 ± 0.05^{ab}	0.59 ± 0.01^{b}
TT80	0.17 ± 0.03^{b}	0.71 ± 0.03^{a}
TT100	0.18 ± 0.07^{b}	0.71 ± 0.05^{a}

Treatment at different temperatures 25 °C (TT25), 40 °C (TT40), 60 °C (TT60), 80 °C (TT80) and 100 °C (TT100). Measurements performed at 25 °C. Means in the same column with different letters are significantly different. Fitting was done on 3 independent measurements.
Different letters in each column denote significant differences between the samples (confidence interval 95%).

Table 3 | Characteristics of the dispersions selected for in vitro gastrointestinal digestion

	$D_{[3,2]}$ (μm)	Viscosity at 40 s^{-1}, 25 °C (Pa s)	Gastric phase (soluble fraction wt%)	Intestinal phase (soluble fraction wt%)
MT60	96.1 ± 3. 1^{a}	Sedimentation	1.00 ± 0.04^{a}	2.15 ± 0.03^{a}
TT25	56.9 ± 0. 3^{b}	0.18 ± 0.06^{a}	0.97 ± 0.01^{a}	2.15 ± 0.03^{a}
TT100	59.1 ± 0. 2^{b}	0.07 ± 0.01^{b}	1.08 ± 0.08^{a}	2.20 ± 0.03^{a}

Particle size $D_{[3,2]}$ of the dispersions and apparent viscosity (40 s^{-1}) at 25 °C. Total solids (wt%) present in the soluble fraction of the gastric and intestinal fluids after digestion. Dispersions were processed by mechanical treatment for 60 s (MT60), mechanical treatment for 90 s at 25 °C (TT25), or by mechanical treatment for 90 s followed by thermal treatment at 100 °C (TT100). Sample MT60 quickly sediments, and the viscosity was not measured. Means in the same column with different letters are significantly different. Analysis was done on 3 independent measurements.
Different letters in each column denote significant differences between the samples (confidence interval 95%).

effect of thermal treatment, *Ulva* spp. dispersions were centrifuged to separate the liquid and dispersed phases.

As shown in Fig. 4B, the liquid phases exhibited Newtonian behaviour with low viscosity (less than one order of magnitude higher than water). Samples treated at 60 °C and above exhibited an increase in the viscosity of the liquid phase, suggesting solubilisation of cellular components. However, this change was not accompanied by a significant variation in total solids content, which remained relatively constant across treatments (1.7–1.8 wt%). This is in agreement with SAXS results, where soluble components could be detected in the liquid phase from thermally treated samples, although the intensity of the shoulder was very weak, suggesting a low concentration of soluble components (Fig. 3B).

This indicates that the increase in viscosity of the liquid phase at higher temperatures is likely due to the solubilisation of higher molecular weight compounds, rather than a greater overall quantity of solubilised material. At 80–100 °C, the viscosity of the dispersions decreased (Fig. 4A), although the viscosity of the liquid phase was higher, indicating that the overall viscosity was primarily governed by the dispersed phase, likely due to particle softening and reduced phase volume.

Regarding the viscoelastic properties (Fig. 4C), G' was higher than G'' for all seaweed dispersions, and they exhibited a slight dependence on frequency, indicating dominant elastic (solid-like) behaviour. Dispersions treated at 40 °C and 60 °C exhibited the highest moduli, with G' values between 7.8–14 Pa for 40 °C and 13–22 Pa for 60 °C, suggesting the formation of a stronger network. In contrast, samples treated at higher temperatures (80 °C and 100 °C) showed a marked decrease in both G' and G'', with G' values dropping to 1–3 Pa, suggesting weakening of the structure. The sample treated at 25 °C displayed intermediate moduli. This behaviour is further supported by tanδ (Fig. 4D), whose value increased sharply at 80 °C and 100 °C. While samples treated at 25 °C, 40 °C, and 60 °C had lower tanδ values (0.25–0.35), indicating predominantly elastic behaviour, samples treated at 80 °C and 100 °C reached values above 0.65, reflecting a transition toward more viscous-dominated behaviour.

Effect of processing on the viscosity of in vitro digested *Ulva* spp. dispersions

For the in vitro gastrointestinal digestion experiments, three dispersions were selected to represent different particle sizes and viscosity (Table 3): MT60, TT25, and TT100. The largest average particle size of 96.1 μm corresponded to MT60, whilst TT25 and TT100, which were either non-thermally treated (TT25) or thermally treated at 100 °C (TT100), had similar $D_{[3,2]}$ with values of 57–59 μm.

Based on the rheological characterisation, TT25 had higher viscosity than TT100, 0.2 Pa s and 0.08 Pa s, respectively. MT60 sedimented quickly,

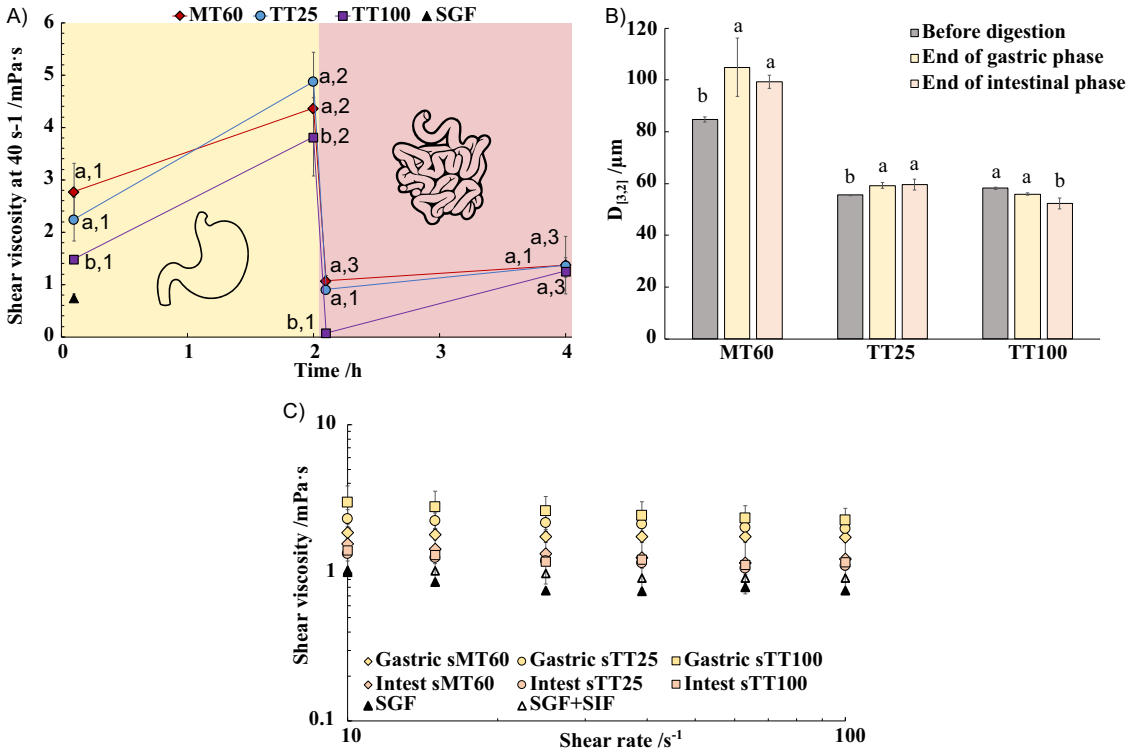

Fig. 5 | Viscosity and particle size evolution during in vitro digestion. A Evolution of the viscosity during in vitro gastrointestinal digestion (37 °C, 40 s^{-1}). Dispersions were mechanically treated for 60 s (MT60), mechanically treated for 90 s at 25 °C (TT25) and mechanically treated for 90 s followed by thermal treatment at 100 °C (TT100). Values within the same time point with different letters differ significantly. Values within the same treatment with different number differ significantly. **B** Evolution of the average particle size $D_{[3,2]}$ during in vitro digestion. **C** Viscosity of the liquid phase of the digesta after the gastric and the intestinal phase. The viscosity of the simulated gastric fluid (SGF) and simulated intestinal fluids (SIF) is also shown for comparison. Average and standard deviation of 6 independent in vitro digestion experiments.

and it was not possible to measure its viscosity. Figure 5A shows that the viscosity of the SGF alone (0.76 mPa s) increased 2–3 fold upon addition of the dispersions. When comparing dispersions with similar particle sizes, TT25, characterised by higher viscosity, resulted in a greater increase in gastric fluid viscosity than TT100, which had lower viscosity.

By the end of the gastric phase (2 h), the viscosity of all samples had increased to 4–5 mPa s and no significant differences were observed between them. In the gastric phase, fruits and vegetables generally lead to an increase in gastric viscosity, primarily due to the hydration and swelling of soluble fibre (e.g., pectin and hemicelluloses) and the presence of insoluble fibre particles. These components can interact with the gastric fluid, forming viscous suspensions that may slow enzyme action and gastric emptying[36].

Similarly, the presence of seaweed particles, rich in fibre, could lead to an increase in gastric viscosity due to swelling, as indicated by the increase in particle size of non-thermally treated samples (MT60 and TT25) depicted in Fig. 5B, likely due to swelling in the gastric environment. Furthermore, polysaccharides such as alginate from brown seaweeds[37] and ulvan[35] present in *Ulva* spp., can form viscous or even gel-like structures under acidic conditions, further enhancing this effect.

As previously discussed, particles in TT100 were already swollen and softer; hence, no further increase in size was observed during the gastric phase for this sample. Although MT60, TT25 and TT100 had different particle sizes and viscosities, the results indicate that the initial differences in viscosity, induced by processing conditions, diminished over time, resulting in no significant differences at the end of the gastric phase.

After 2 h, the samples were mixed with simulated intestinal fluid (SIF) to progress into the intestinal phase, and the viscosity immediately decreased to 0.1–0.9 Pa s due to the dilution with SIF, bile and pancreatic enzymes. For MT60 and TT25, the viscosity remained rather stable until the end (Fig. 5A). However, for TT100, the viscosity increased significantly during the intestinal phase. This indicates that during the intestinal phase, enzymatic activity and the increase in pH did not result in the solubilisation of cell components that significantly increased viscosity in MT60 and TT25; nevertheless, such an effect was observed in TT100.

Figure 5B showed that the particle size did not change during the intestinal phase for the non-thermally treated samples; however, a decrease in size was observed for the thermally treated TT100. This could be explained by the presence of softer particles with cell walls that are more accessible to enzymatic action in the thermally treated sample, enhancing structural changes during digestion, which, on the one hand, increases the viscosity of the digesta and, on the other hand, reduces particle size.

The solid fraction of the digesta, which contains the insoluble non-digestible materials, and the liquid fraction containing soluble digestible components, were separated by centrifugating the gastric and intestinal phases. The viscosity of the soluble fraction after the intestinal phase was lower than after the gastric phase (Fig. 5C); even so, it contained a higher concentration of soluble solids (Table 3), from intestinal salts and enzymes present in the SIF, as well as digestion products, whose contribution to the viscosity is minor, likely due to their lower molecular weight.

After the gastric phase, the average particle size remained large (50–100 µm) (Fig. 5B) and intracellular contents were still retained within the cells. This was visualised in CLSM images before digestion (Fig. 6A, B), and after the gastric phase (Fig. 6C, D), suggesting that the pH and enzymatic reactions in the stomach were not enough to break *Ulva* spp. tissues or permeabilised seaweed cells. Even after a thermal treatment at 100 °C, cell content was still observed inside the cells (Fig. 6D). Similarly, after the intestinal phase, the particle size was large (Fig. 5B).

Although no quantification was performed, CSLM images appeared to show that thermally treated samples had more empty cells and that their cell walls were thinner and more disrupted (Fig. 6F) compared to unheated samples (Fig. 6E). This observation is relevant from a nutritional point of view as only solubilised components would be absorbed in the stomach and

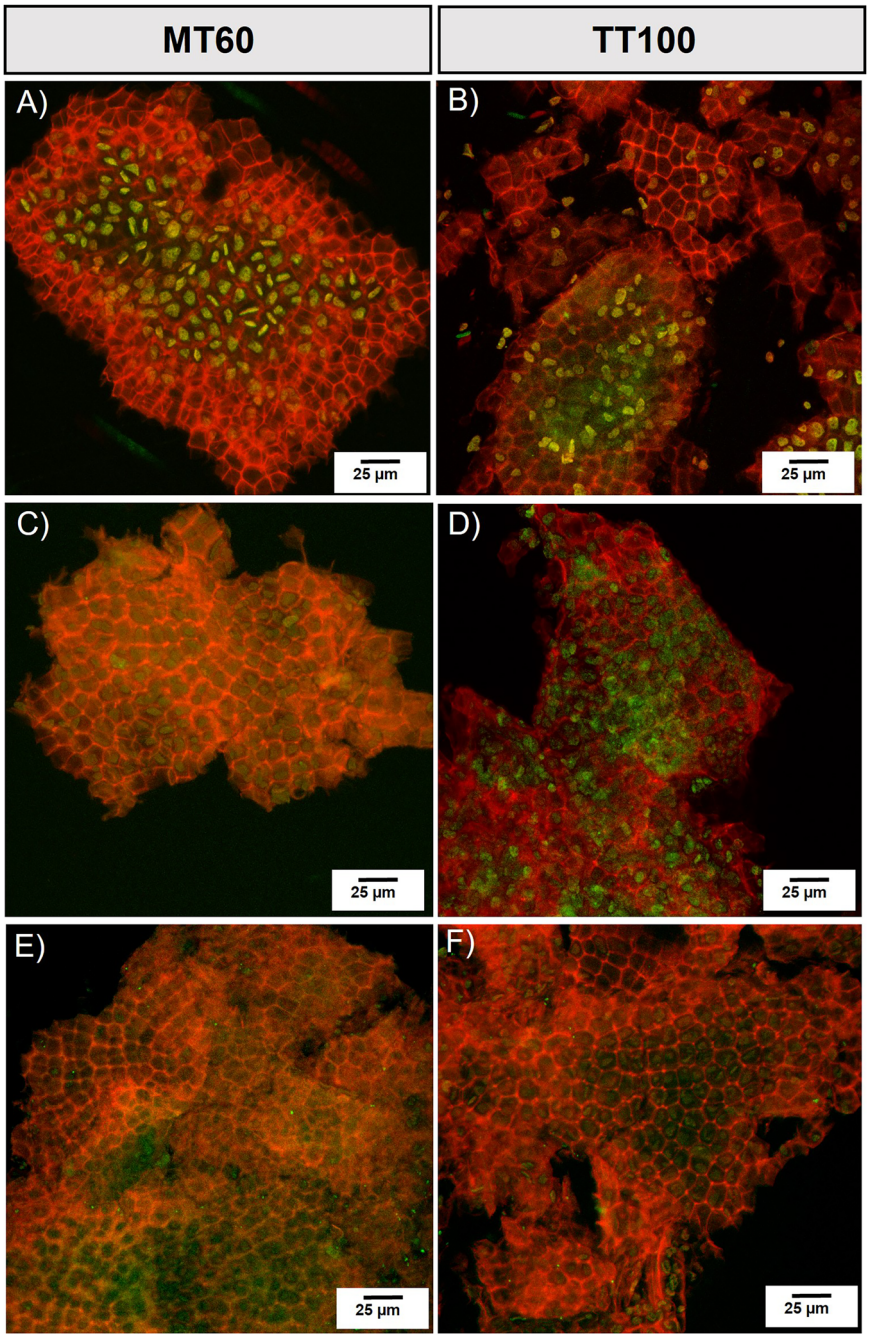

Fig. 6 | Structural features in Ulva tissue after in vitro digestion. Confocal laser scanning microscopy (CLSM) images of the dispersions before in vitro simulated digestion (**A**, **B**), after the gastric phase (**C**, **D**) and after the small intestinal phase (**E**, **F**). Samples are stained with Congo red, showing cell wall polysaccharides (in red), and an autofluorescence signal coming from intracellular content was also recorded (in green).

small intestine, whilst undigested material would go all the way to the large intestine where they will be fermented by gut microbiota.

Nanostructural modifications in *Ulva* spp. cell walls induced by in vitro digestion

SAXS experiments were performed on both the soluble and insoluble fractions of the digesta, which were separated by centrifugation. Although the samples have added complexity, SAXS can provide reliable information on insoluble material because it detects X-ray scattering from electron density contrasts, regardless of whether the material is soluble[32,38]. SAXS revealed significant nanostructural differences in the solid insoluble fraction and the liquid soluble fraction of the digesta as function of processing conditions (Fig. 7). In the dispersion with the largest particle size (MT60) the structure of the cell wall remained largely intact after the gastric phase (Gast. iMT60), with the peak at 0.14 $Å^{-1}$, corresponding to cellulose microfibrils, and the shoulder at 0.06 $Å^{-1}$, attributed to xylose domains interacting with cellulose, still present at the end of the gastric phase. Even so, the shoulder shifted towards higher q, suggesting that a fraction of ulvan might have been solubilised upon digestion.

A similar effect was observed for the TT25 sample, suggesting that no major cell wall nanostructural changes occurred during the gastric phase. In the case of the sample treated at the highest temperature (TT100), a more evident change was observed in the shoulder feature after the gastric phase, indicating that ulvan might have been solubilised to a greater extent in that case. After the intestinal phase, the cellulose peak was not visible in the scattering pattern from the insoluble fraction of MT60 (Intest. iMT60), and instead, a much more intense and defined peak located at 0.13 $Å^{-1}$ was visible.

The same peak, although much less intense and defined, was also observed in the intestinal soluble fraction (Intest. sMT60). This peak is

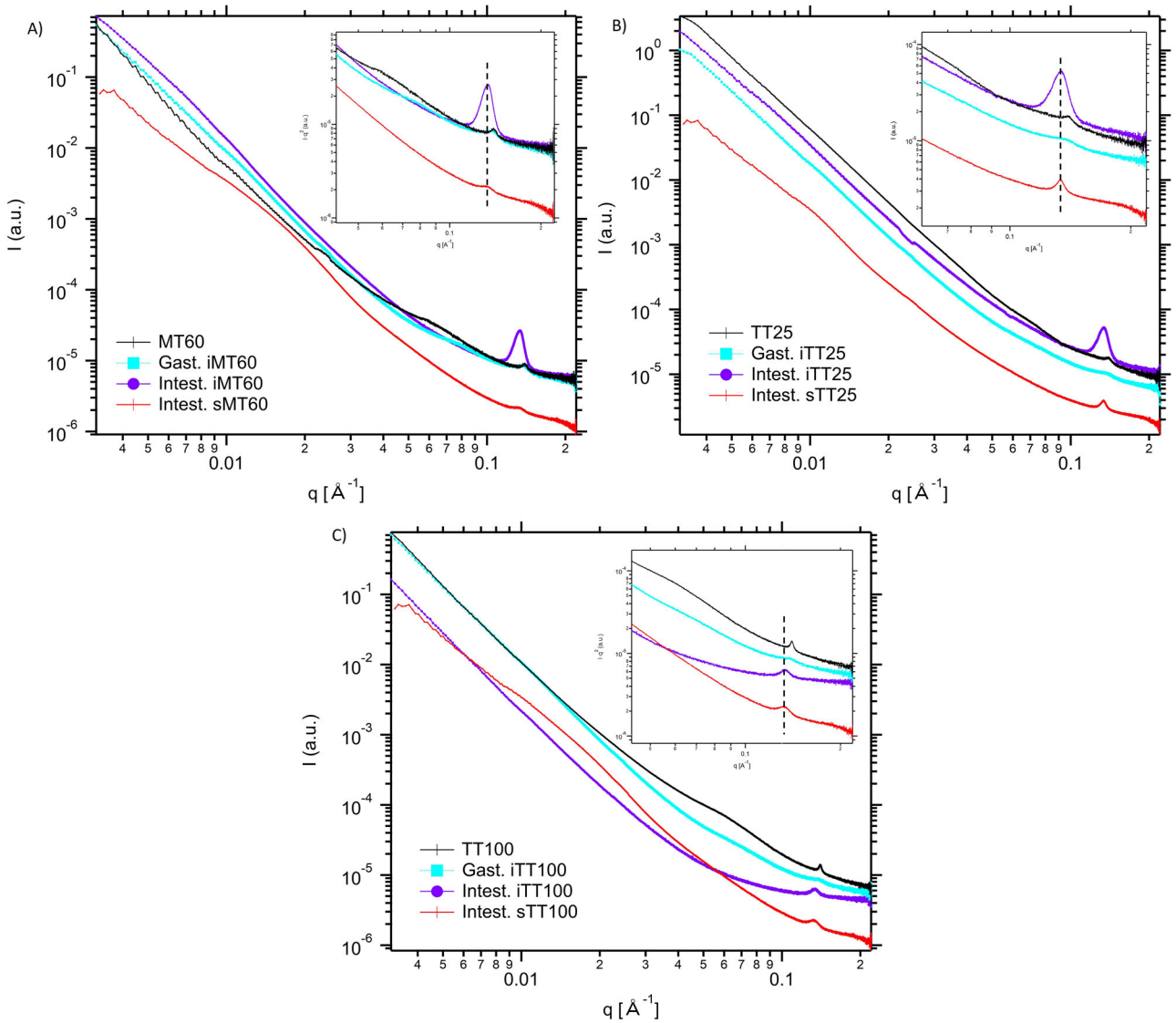

Fig. 7 | Nanostructural features in the digesta detected by Small angle X-ray scattering (SAXS). SAXS patterns of in vitro digested *Ulva* spp. MT60 (**A**), TT25 (**B**) and TT100 (**C**) dispersions. The insoluble (i) and soluble fractions (s) obtained at the end of the gastric and intestinal phase are shown. The insoluble fraction was analysed and dried. The SAXS pattern of the dispersion prior to in vitro digestion is shown for comparison (MT60, TT25, TT100).

attributed to the formation of ordered micellar/lamellar structures by bile salts. It should be noted that the appearance of this intense peak in the insoluble fraction masks the weak peak from cellulose microfibrils, since they overlap. Thus, it is not possible to draw conclusions from the effect of the intestinal digestion phase on the structure of cellulose. The same peaks attributed to bile salts were observed in the intestinal soluble and insoluble fractions from the TT25 and TT100 samples, although interestingly, the intensity of the peak in the insoluble fraction was decreased, especially in TT100, while the peak became more intense in the soluble fractions. It has been previously demonstrated that some soluble polysaccharides, as well as peptides released upon digestion of proteins, can interact with bile salts, affecting their structural arrangement, either disrupting or stabilising them[39,40].

The fact that a larger proportion of bile salt structures remained in the insoluble fraction from MT60 might be related to a lower degree of hydrolysis and release of components, such as soluble polysaccharides and peptides, during digestion. In that case, very low concentrations of soluble components are found in the digestion medium, and therefore, most of the bile salt structures remain intact and precipitate. In contrast, a greater degree of hydrolysis and solubilisation of components in TT25, and especially in TT100, favours the interactions of these components with bile salts, destabilising their native micellar/lamellar structures and forming mixed nanostructures in the soluble fraction. In addition to the bile salts peak, a broad shoulder was detected in the low q region of the soluble fractions from all the samples. This shoulder feature was centred at ca. 0.011–0.016 Å^{-1}, corresponding to a real distance of ca. 39 nm, hence suggesting that larger structures were also generated upon digestion, which could most likely be explained by the solubilisation of ulvan, as noted in the SAXS patterns from thermally treated samples (Fig. 3B). These results suggest that samples thermally treated (TT100) are easier to digest than non-thermally treated samples. Similarly, samples with a smaller particle size (TT25) are easier to digest than samples with a larger particle size (MT60).

Discussion

Processing conditions influenced the structural disruption of *Ulva* tissue and the rheological properties of the resulting dispersions. Mechanical treatment primarily affected particle size distribution (Fig. 1B), as shear forces physically broke down the tissue and increased the surface area available for further degradation. In contrast, thermal treatment impacted cell wall integrity and promoted the solubilisation of intracellular and cell wall components, increasing the viscosity of the liquid phase (Fig. 4B).

The molar mass of the solubilised polysaccharides may vary depending on the processing conditions. Thermal treatment, in particular, can partially degrade or break down polysaccharide chains. Ulvans are typically extracted at temperatures around 90 °C and remain stable up to approximately 180 °C[41,42]. From a nutritional point of view, thermal treatments may also influence thermo-labile nutrients present in *Ulva*, such as vitamin C, some B vitamins, and proteinase inhibitors; however, these compositional aspects were beyond the scope of the present study.

The effect of thermal and mechanical treatments was evident across length scales. At the microscale, clusters of intact and partially intact cells containing retained cellular material were observable via confocal scanning laser microscopy (CSLM), regardless of treatment intensity (Fig. 2). However, SAXS analysis revealed nanoscale disruption of cell walls (Fig. 3A), with evidence of ulvan being released into the continuous phase (Fig. 3B), contributing to increased viscosity.

Rheologically, the viscosity of the dispersion depends on both the volume fraction occupied by the dispersed phase and the viscosity of the continuous phase. While ulvan solubilisation at 80 °C[43,44] likely contributed to increased liquid phase viscosity (Fig. 4B), this effect was insufficient to fully offset the decrease in volume of the dispersed phase resulting from thermal softening of particles. Notably, not all ulvan fully dissolved, but a certain fraction remained partially associated with the cell wall (Fig. 3A), swelling and forming softer particles, leading to an increased particle deformability resulting in dispersions with lower viscosity (Fig. 4A) and weaker network structure (Fig. 4C, D).

At higher processing temperatures (above 80 °C), SAXS suggested a certain degree of phase separation within the cell wall, with denser cellulose-rich domains coexisting alongside more swollen cellulose-xylose regions (Fig. 3A). Given that cellulose comprises only ~15% of the *Ulva* cell wall (Table 1), it is likely that ulvan, which accounts for over 50% of the polysaccharide content, plays a dominant role in promoting particle softening and flexibility through hydration and gelation[45]. Elasticity in a dispersion of soft particles (such as seaweed cellular structures) arises primarily from the formation of a percolated network of hydrated, flexible particles that interact through physical entanglements, electrostatic interactions, and hydrogen bonding[46,47]. In such systems, the dispersed seaweed particles, which are rich in polysaccharides such as ulvan, can swell and form a soft, gel-like matrix. When these particles are present at sufficient concentrations, they come into close proximity, allowing for transient connections that resist deformation under applied stress.

These interactions create a viscoelastic network capable of storing mechanical energy, which is manifested as the storage modulus (G'), as previously described for suspensions of plant material[48,49]. The degree of elasticity depends on factors such as particle size and surface, degree of swelling, and the nature of the solubilised biopolymers in the liquid phase. Since the particle size, charge, and total solids concentration across the samples was similar, and the viscosity of the liquid phase decreased only slightly at 80 °C and 100 °C, we proposed that the reduced elasticity observed at 80 °C and 100 °C can be attributed mainly to thermal effects on the particle structure, i.e. softening of the seaweed particles, through higher swelling of ulvan rich domains, collapse of cellulose microfibrils and phase separation in their cell walls, as described above. Softer particles are more prone to deformation, which compromises the integrity of the interparticle network.

As a result, the ability of the dispersed phase to store elastic energy (G') is diminished, and the system transitions toward more viscous, less elastic behaviour. Thus, structural changes (Fig. 3) are consistent with the observed reduction in G' of the dispersions treated at 80 °C and 100 °C (Fig. 4C, D), which reflects a softer material. Together, our results showed that moderate heating (40–60 °C) enhances network strength, while intense heating (above 80 °C) compromises the structural integrity of *Ulva* spp. dispersions. This demonstrates that dispersion structure and rheology can be tailored through controlled processing, allowing the design of seaweed-based materials with diverse textural properties.

Importantly, such structural and rheological modifications also had implications for digestion. Particle size and viscosity are both critical factors in modulating digestive kinetics. Smaller particles present greater surface area for enzymatic action, whereas increased viscosity can reduce enzyme diffusion and delay gastric emptying. This is particularly relevant for fibre-rich foods such as *Ulva* spp., in which soluble fibres, such as ulvan, could contribute significantly to digesta viscosity.

During the gastric phase, swelling of seaweed particles was observed in non-thermally treated samples MT60 and TT25, reflected by an increase in particle size (Fig. 5B) and nanostructural changes measured by SAXS (Fig. 7A, B). In contrast, TT100, which was thermally treated, showed no change in particle size (Fig. 5B), but SAXS revealed that ulvans might have been solubilised to a greater extent during the gastric phase. The swelling and hydration of cell walls could contribute to the observed increase in digesta viscosity (Fig. 5A) of MT60 and TT25, as observed for fruits and vegetables due to pectins and hemicelluloses present in their cell walls[36]. Furthermore, polysaccharides like alginate and ulvan have been reported to form viscous or gel-like networks under acidic conditions[35,37], reinforcing this viscosity increase, as observed for TT100. Although initial gastric viscosities varied across treatments and were correlated to the initial dispersion viscosity, these differences disappeared during digestion, with no significant viscosity differences at the end of the gastric phase (Fig. 5A). At gastric pH, the carboxyl and sulphate groups of ulvan might become protonated, reducing electrostatic repulsion and solubility, which promotes aggregation[50]. It is plausible that dispersions with higher viscosities than the ones studied here could exhibit different digestive behaviours[51], more viscous systems might be more resistant to breakdown and mixing in the gastric environment.

These results indicate that the thermally treated dispersion TT100, which had the lowest initial viscosity, contained softened seaweed particles that were more susceptible to gastric changes, including solubilisation of cell wall polysaccharides and enzymatic hydrolysis of starch and proteins. This led to a greater increase in viscosity during gastric digestion compared to dispersions with higher initial viscosity (Fig. 5A). The minor (or absent) particle size reduction during the intestinal phase across treatments (Fig. 5B), also visualised in CLSM images (Fig. 6), suggests that structural changes at the nanoscale, rather than microscale breakdown, govern digestion behaviour. Greater structural disruption is expected to correlate with enhanced release of cellular contents. Among the tested samples, the thermally treated sample TT100 exhibited the highest degree of structural changes. This sample showed a viscosity (0.07 mPa s), which lies very close to the 0.1 mPa s threshold reported in the literature as the point at which viscosity begins to hinder digestibility [19] Being just below this critical value suggests that TT100 remains sufficiently fluid to allow efficient enzyme mixing and substrate interaction, which may lead to higher bioaccessibility and potentially greater bioavailability.

SAXS data (Fig. 7A)indicated that in MT60, limited solubilisation during digestion resulted in more intact bile salt micellar/lamellar structures accumulating in the insoluble fraction, likely due to insufficient release of peptides and polysaccharides to interact with bile salts. In contrast, greater solubilisation observed in TT100, also reflected by the increased viscosity during the intestinal phase (Fig. 5A), suggests enhanced hydrolysis and release of ulvan and other soluble components, e.g. protein and lipids. These components likely disrupted bile salt assemblies, forming mixed nanostructures detectable in the soluble fraction (Fig. 7C)[52]. The combination of reduced particle size and thermal treatment in TT25, and especially TT100, thus appears to promote the formation of digestion-relevant nanostructures and improve matrix breakdown.

While we did not directly measure the bioaccessibility or bioavailability of nutrients, our analyses allow us to infer that the solid phase, which consists of insoluble, recalcitrant seaweed material, remains structurally resistant and is therefore expected to reach the large intestine for fermentation, whereas the material in the liquid phase is likely absorbable and thus potentially available for uptake. Seaweed-derived compounds, such as dietary fibre, can interact directly with the gut microbiota, influencing both its composition and bacterial diversity[8,53]. Through microbial fermentation

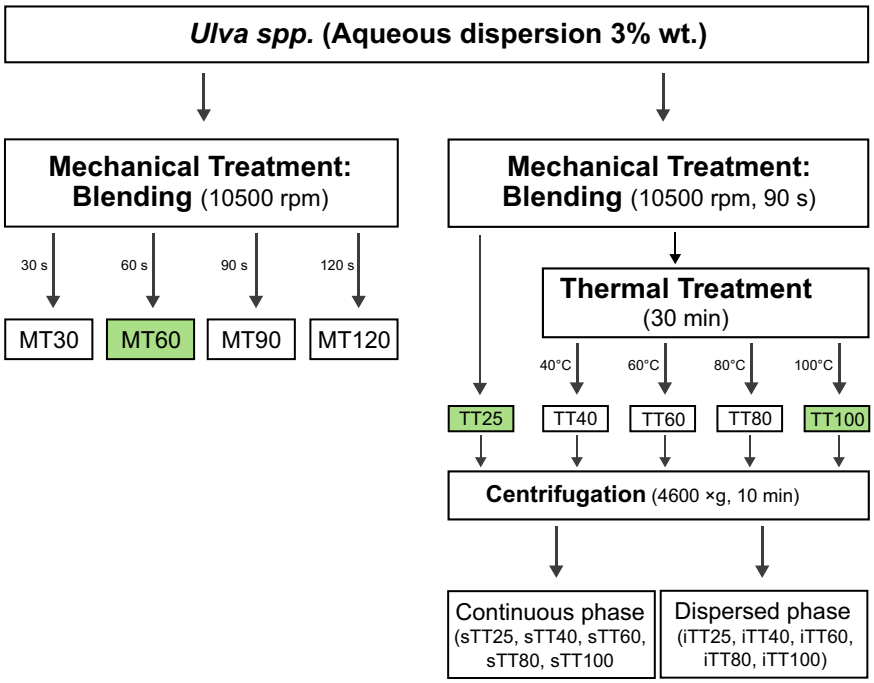

Fig. 8 | Overview of the processing workflow and corresponding sample codes. Samples highlighted in green were subjected to INFOGEST in vitro digestion.

and transformation, these components may give rise to bioactive metabolites such as short-chain fatty acids (SCFAs), which exert systemic effects on immune modulation, metabolic regulation, and even gut–brain signalling[54]. Therefore, the fibre present in the solid phase of the digesta may contribute to health outcomes via microbiota-mediated mechanisms in the large intestine, a hypothesis that warrants further investigation in both mechanistic and clinical studies. Our study provides initial insights into structural changes of *Ulva* seaweed during digestion, but does not capture the full physiological context. Validation through in vivo studies is needed to assess nutrient absorption across processing methods, and to complete the digestive cycle with gut fermentation studies quantifying short-chain fatty acids and microbiota profile.

This study demonstrates that conventional processing methods, such as blending and heating in water, can effectively modulate the structure and rheology of green seaweed *Ulva* spp. dispersions, with potential implications for gastrointestinal digestion. Our findings highlight how processing conditions affect both insoluble and soluble phases, influencing digesta structure and flow behaviour during digestion. Gastric and small intestinal digesta are complex fluids containing undigested seaweed particles (cell clusters and single cells) and dissolved cellular components. Despite similar final digesta viscosities, small-angle X-ray (SAXS) experiments revealed clear differences in structural degradation, i.e. samples with larger particle sizes retained more intact cell walls, whereas heat-treated samples were more extensively broken down, indicating higher digestibility.

These findings show the importance of combining structural and rheological measurements to fully understand the digestive behaviour of seaweed-based foods. Whilst SAXS provides information about cell wall disassembly, viscosity data offer complementary insights into the physical properties of the digesta. The low viscosity observed during the gastric phase suggests that the studied *Ulva* spp. dispersions are unlikely to hinder gastric emptying or mixing with digestive enzymes, which are important factors for efficient digestion and nutrient bioaccessibility. These results highlight the need for optimised processing strategies to enhance both the structural breakdown and favourable rheological properties of green seaweed, ultimately supporting its application in the development of functional and nutritious seaweed-based food products.

Methods

Raw material

The green macroalgae *Ulva* spp. were provided by the company Porto-Muiños (A Coruña, Spain). It was collected from the Atlantic Ocean off the coast of A Coruña (Spain) during the autumn-winter season in 2022. After collection, the seaweeds were frozen at −20 °C and transported frozen. Upon arrival at the lab, the biomass was stored at −20 °C.

Preparation of seaweed dispersions

Seaweed was thawed overnight and washed under running water to remove impurities prior to the experiments. Based on preliminary trials, to obtain dispersions with a concentration of 3% w/w, the seaweed was mixed with water in a ratio 1:3. First, the mechanical impact was evaluated by blending the seaweed/water mixture in a food processor (Thermomix TM6, Vowerk, Germany) at maximum speed (10,500 rpm) for 30, 60, 90 and 120 s. In a second experiment, the impact of heat was assessed by preparing a large batch (2 L) mixed for 90 s, which was then divided into four subsets. These subsets were thermally treated in a water bath at 40, 60, 80 and 100 °C for 30 min with constant agitation and covered to reduce evaporation. A control sample without thermal treatment (25 °C) was also included. The liquid (continuous) and solid (dispersed) phases of the dispersions were separated by centrifugation at 4600×*g* for 10 min. Processing workflow and sample codes are shown in Fig. 8.

In vitro simulated gastrointestinal digestion

In vitro simulated gastrointestinal digestion was carried out based on the INFOGEST protocol[55] with some modifications. We focus on dispersions with different particle sizes (MT60, TT25) and, with or without thermal treatment (TT25 and TT100).

The oral phase was omitted due to the low viscosity of the samples, which would result in a very rapid oral transit, minimising dilution, adhesion, and contact with saliva. This decision was supported by the INFOGEST protocol[55,56] and by previous studies on seaweed-based systems that also excluded this step[57,58].

Samples (10 mL) were diluted 1:1 (v/v) with simulated gastric fluid (SGF) at pH 3 containing porcine pepsin (2000 U/mL) (Sigma-Aldrich, St. Louis, USA) and incubated with agitation for 2 h at 37 °C. The reaction was stopped by adjusting the pH to 7 with 1 M NaOH, obtaining the gastric

digesta. For the intestinal phase, another set of samples was prepared as described above, but after 2 h instead of adding NaOH they were further diluted 1:1 (v/v) with simulated intestinal fluid at pH 7 containing pancreatin (100 U/mL) (Sigma-Aldrich, St. Louis, USA) and bovine bile extract (10 mM) (Sigma-Aldrich, St. Louis, USA), followed by a 2 h incubation with agitation at 37 °C. Sampling was performed at four time points: initially (time 0), at the end of the gastric phase (2 h), immediately after mixing with the simulated intestinal phase, and at the end of the intestinal phase (4 h). After each digestion stage (gastric and gastric + intestinal), algae dispersions were separated into liquid and solid fractions by centrifugation at 4600×*g* for 10 min. Liquid fractions are considered bioavailable and absorbable in the intestine, while solid fractions represent non-digestible material. Controls without seaweed dispersion (SGF, SGF + SIF) underwent the same procedure, and the viscosity was also measured. Samples were stored at 4 °C until further analysis. Each digestion was performed in triplicate.

Dry matter

The total solids content of the raw material, the dispersions and soluble fractions of undigested and digested samples were measured by drying the samples in an oven at 100 °C for 24 h, then they were cooled down in a desiccator and weighed again. The difference in weight indicates the dry matter. Samples were prepared in triplicate.

Total protein

The protein content was determined using the Kjeldahl method[59]. Each sample (5 g) was prepared in duplicate. Samples were transferred to digestion tubes, with each tube containing two glass beads and two copper sulfate tablets ($CuSO_4$–$5H_2O$), and 10–15 mL of 96% sulfuric acid was added. The digestion unit (Kjeldatherm, Gerhardt, Königswinter, Germany) was set at 420 °C for 2 h, then cooled for at least 1 h. During distillation, 50 mL of distilled water and 50 mL of NaOH (50%) solution were added to each tube. The resulting distillate was collected in a flask with 30 mL of boric acid (H_3BO_3) 4% w/w and a Kjeldahl indicator. The sample was titrated with HCl (0.1 N). HCl volume was recorded to calculate N content and converted to protein using a factor of 5.13[60].

Total fat

The fat content was determined following the standard method Schmid–Bondzynski–Ratzalff[61]. Sample (1 g) was weighed and placed in Mojonnier extraction tubes, and 8–10 mL of HCl was added. The mixture was gently heated with a Bunsen burner. Subsequently, 10 mL of ethanol, 25 mL of diethyl ether, and 15 mL of petroleum ether were added. The mixture was agitated, releasing gas as needed. After phase separation, the upper fat-containing layer was decanted into beakers. This process was repeated three times. Fat fractions were evaporated at 100 °C in an oven for 1 h, then cooled in a desiccator and weighed. A blank was also included. Samples were measured in triplicate.

Total fibre

The Total Dietary Fibre Assay Kit (Megazyme) was used for the analysis of Total Fibre. In brief, total dietary fibre (TDF) was determined on duplicate samples of dried and defatted material based on the AOAC method 985.29. Samples were cooked at 100 °C with heat-stable *α*-amylase to induce gelatinisation, hydrolysis and depolymerisation of starch; incubated at 60 °C with protease (to solubilise and depolymerise proteins) and amyloglucosidase (to hydrolyse starch fragments to glucose); and treated with four volumes of ethanol to precipitate soluble fibre and remove depolymerised protein and glucose. The residue is filtered, then washed with 78% ethanol, 95% ethanol, and acetone; dried and weighed. One duplicate is analysed for protein, and the other is incubated at 525 °C to determine ash. The TDF is the weight of the filtered and dried residue minus the weight of the protein and ash.

Ash content

Samples were placed in pre-weighed, dried ceramic crucibles. Samples were dried at 100 °C for 1 h, then incinerated in a furnace at 500 °C for 4 h. After cooling in a desiccator, samples were weighed again and the ash content calculated as the difference in weight. Samples were measured in triplicate.

Monosaccharide analysis

The monosaccharide composition was determined in the *Ulva* spp. seaweed by two-step methanolysis using 50 mg of the sample. Samples were treated at 100 °C for 5 h with 5 mL of 2 M HCl, neutralised with pyridine, then mixed with 5 mL of 2 M trifluoroacetic acid (TFA) and autoclaved for 1 h at 120 °C. Duplicates of each sample were hydrolysed. The samples were filtered using 0.2 µm nylon filters [23,62], diluted to a volume of 10 mL, of which 20 µL were injected into an ionic chromatographer with pulsed amperometric detection system (Metrohm 930 IC Flex, Metrohm Hispania, Madrid, Spain), equipped with a Metrosep Carb 2 column (4 × 250 mm, Metrohm). The mobile phase was a mixture of NaOH (180 mM) and sodium acetate (300 mM) with a flow of 0.6 mL min^{-1} and a gradient to 50%.

The monosaccharide standards used were Gal (Galactose standard for IC); Glu (Glucose standard for IC); Xyl (Xylose standard for IC); Man (D-(+)-Mannose-analytical standard); Rham (Rhamnose standard for IC); GlcA (D-glucuronic acid) and IdoA (Iduronic acid). All standards were from Supelco (Bellefonte, USA) except GlcA, which was from BLDPharm (BLD Pharmatech Ltd., Shanghai, China) and IdoA (L-Iduronic acid sodium salt) from Biosynth (Staad, Switzerland). The standard mixtures (4 in total) were prepared with concentrations of 1, 2, 5 and 10 mg L^{-1} for all monosaccharides.

Particle size characterisation

Particle size measurements were conducted using a particle size analyser (Mastersizer Hydro 2000SM, Malvern Instruments, Worcestershire, UK). Approximately 0.5 mL of seaweed aqueous dispersion was added into a small sample volume dispersion unit (Malvern Instruments, Worcestershire, United Kingdom) filled with deionised water under continuous agitation (3000 rpm). The refractive index was set at 1.46 with an absorption value of 0.01, and water was used as the dispersant. The laser obscuration range was set between 5% and 10%. Due to the heterogeneous morphology of the particles, the "irregular shape" option was chosen in the software. The particle size distribution was calculated using the instrument software (Mastersizer 2000, Malvern Instruments, Worcestershire, UK) from the dispersed light intensity profile. In highly polydisperse systems, such as these seaweed dispersions, the surface-based diameter $D_{[3,\ 2]}$ is chosen as the indicator of the average particle size [63].

ζ potential measurements

The ζ potential of the dispersions (at their native pH) was measured using a Zetasizer Nano ZS (Malvern Instruments Ltd., Worcestershire, UK). A 0.1 mg/mL dispersion was analysed. The cuvette used for the measurement was a folded capillary zeta cell (Malvern Instruments Ltd., Worcestershire, UK). All samples were done in triplicate with 1–100 subruns.

Microscopy

The microstructure of the processed seaweed dispersions was examined using an optical microscope (Olympus BX50F4 Epifluorescence), equipped with a CCD camera. Samples were diluted with Milli-Q water, and a few drops were mounted on glass slides and covered with cover slips. Observations were carried out using 10× and 40× air objectives, with a minimum of six images captured at each magnification.

Confocal laser scanning microscopy (CSLM) was also used to visualise the microstructure of seaweed dispersions. Cell walls were stained with Congo Red. A couple of drops of Congo red (1 wt%) were mixed with 2mL of the dispersion, washed twice and placed on microscopic slides covered with coverslips. Confocal images were acquired using an upright laser scanning microscope SPE with a ACS-APO 20×/NA 0.6 objective (Leica Microsystems, Wetzlar, Germany). Green fluorescence was acquired by exciting samples with a 488 nm laser, and the emission signal was detected between 491 and 573 nm. Red fluorescence from Congo Red was acquired

by exciting samples with a 561 nm laser, and the emission signal was detected between 583 and 681 nm. Sequential scanning mode was used to avoid crosstalk between channels. All images shown correspond to a maximal intensity projection of a confocal z-stack. Images were processed with LasX and Adobe Photoshop CS.

Small angle X-ray scattering (SAXS)

SAXS experiments were carried out in the Non Crystalline Diffraction beamline, BL-11, at the ALBA synchrotron light source in Spain[64]. The seaweed powders and the aqueous dispersions obtained after the thermal and mechanical treatments, as well as their respective serum phases, were placed into sealed 2 mm quartz capillaries (Hilgenberg GmbH, Germany) and analysed. The energy of the incident photons was 12.4 keV or equivalently a wavelength, λ, of 1. The SAXS scattering patterns were collected by means of a photon counting detector, Pilatus 1 M 3S, with an active area of 168.7×179.4 mm^2, an effective pixel size of 172×172 μm^2 and a dynamic range of 20 bits.

The sample-to-detector distance was set to 6695 mm, resulting in a q range with a maximum value of $q = 0.2$ Å^{-1}. An exposure time of 10 s was selected based on preliminary trials. The data reduction was treated by the pyFAI Python code (ESRF)[65], modified by ALBA beamline staff, to do online azimuthal integrations from a previously calibrated file. The calibration files were created from a silver behenate (AgBh) standard. The intensity profiles were then represented as a function of q using the IRENA macro suite[66] within the Igor software package (Wavemetrics, Lake Oswego, Oregon).

Rheological properties

To assess the rheological properties of the dispersions, a rheometer (Discovery HR20, TA Instruments, Delaware, USA) was configured with a solvent trap parallel plate stainless steel setup (40 mm diameter). A gap of 1 mm was selected. To evaluate rheological properties relevant for product development and stability, measurements were conducted at 25 ± 0. 1 °C, maintained with a Peltier system. To determine the viscoelastic behaviour, an angular frequency sweep from 0.6 to 50 rad s^{-1} was applied at a constant strain of 1%, selected within the linear viscoelastic region (LVR). The LVR was determined by performing a strain sweep from 0.01 to 1000% with an angular frequency of 10 rad s^{-1}. Samples were analysed in triplicate, loading a fresh sample for each measurement. Storage modulus (G'), loss modulus (G'') and tanδ (Eq. (1)) were obtained.

$$\mathrm{Tan}\delta = \frac{G''}{G'} \tag{1}$$

For viscosity measurements, a steady state measurement with logarithmically increasing shear rate from 0.1 to 100 s^{-1} was applied. Samples were measured in triplicate. Flow curves were fitted to a power law model (Eq. (2)) to determine consistency and flow behaviour index of the dispersions:

$$\sigma = K\dot{\gamma}^n \tag{2}$$

With σ representing the shear stress (Pa), $\dot{\gamma}$ is the shear rate (s^{-1}), K the consistency coefficient (Pa s^n), and n the flow behaviour index.

The viscosity of the liquid phase was measured using a stainless steel cone geometry (40 mm) with a 2° angle. A shear rate sweep from 1 s^{-1} to 100 s^{-1} was applied at 25 °C.

To measure the viscosity of the in vitro digested samples, the parallel plates were used, whereas for the gastrointestinal juices, the cone geometry was selected. The same experimental conditions described above for dispersions and the liquid phase were used. Measurements were performed at 37 °C to simulate the biological temperature of the digestive process. All measurements were performed in triplicate.

Statistical analysis

One-way ANOVA was employed to evaluate the effect of treatment on particle size and on tanδ. Tukey's test was used to compare variations (confidence interval of 95%). Two-way ANOVA was employed to evaluate differences in digesta over time and as a function of processing conditions. Tukey's contrast test was used to compare differences in treatments and timing. "R" was the open software used for all statistical analysis[67].

Data availability

Data is provided within the manuscript or supplementary information files.

Received: 19 May 2025; Accepted: 11 November 2025;
Published online: 24 November 2025

References

1. Juul, L. et al. Ulva species: A critical review on the green seaweed as a source of food protein. *Trends Food Sci. Technol.* **149**, 104534 (2024).
2. Salido, M., Soto, M. & Seoane, S. Seaweed: nutritional and gastronomic perspective. A review. *Algal Res.* **77**, 103357 (2024).
3. Juul, L. et al. Combining pressing and alkaline extraction to increase protein yield from ulva fenestrata biomass. *Food Bioprod. Process.* **134**, 80–85 (2022).
4. Kazir, M. & Livney, Y. D. Plant-based seafood analogs. *Molecules* **26**, 1559 (2021).
5. Vega-Gomez, L. M. et al. Production of hybrid protein-polysaccharide extracts from Ulva spp. seaweed with potential as food ingredients. *Food Hydrocoll.* **153**, 110046 (2024).
6. Nissen, S. H., Juul, L., Bruhn, A., Sondergaard, J. & Dalsgaard, T. K. The biochemical composition and its relation to color of Ulva spp. upon harvest time. *J. Appl. Phycol.* **36**, 2095–2107 (2024).
7. Corino, C., Prost, M., Pizzi, B. & Rossi, R. Dietary plant extracts improve the antioxidant reserves in weaned piglets. *Antioxidants* **10**, 702 (2021).
8. Shannon, E., Conlon, M. & Hayes, M. Seaweed components as potential modulators of the gut microbiota. *Mar. Drugs* **19**, 358 (2021).
9. Molina-Gilarranz, I., Cebrián-Lloret, V., Recio, I. & Martínez-Sanz, M. Impact of structure and composition on the digestibility and nutritional quality of alternative protein-rich extracts from the green seaweed Ulva lacinulata. *Food Res. Int.* **201**, 115646 (2025).
10. Trigo, J. P. et al. In vitro digestibility and CaCo-2 cell bioavailability of sea lettuce (Ulva fenestrata) proteins extracted using ph-shift processing. *Food Chem.* **356**, 129683 (2021).
11. Pootthachaya, P. et al. Investigation of nutritional profile, protein solubility and in vitro digestibility of various algae species as an alternative protein source for poultry feed. *Algal Res.* **72**, 103147 (2023).
12. Mišurcová, L. *Seaweed Digestibility and Methods used for Digestibility Determination*, chap. 13, 285–301 (John Wiley & Sons, Ltd., 2011).
13. Cebrián-Lloret, V., Martínez-Abad, A., Recio, I., López-Rubio, A. & Martínez-Sanz, M. In vitro digestibility of proteins from red seaweeds: Impact of cell wall structure and processing methods. *Food Res. Int.* **178**, 113990 (2024).
14. Azaza, M. S., Dhraief, M. N., Kraiem, M. M. & Baras, E. Influences of food particle size on growth, size heterogeneity, food intake and gastric evacuation in juvenile Nile tilapia, Ooreochromis niloticus, l., 1758. *Aquaculture* **309**, 193–202 (2010).
15. de Oliveira, M. N. et al. Nutritive and non-nutritive attributes of washed-up seaweeds from the coast of Ceara, Brazil. *Food Chem.* **115**, 254–259 (2009).
16. Bikker, P. et al. Biorefinery of the green seaweed Ulva lactuca to produce animal feed, chemicals and biofuels. *J. Appl. Phycol.* **28**, 3511 (2016).

17. Ribeiro, D. M. et al. Piglets performance, nutrient digestibility and gut health in response to feeding *Ulva lactuca* seaweed supplemented with a recombinant Ulvan lyase or a commercial carbohydrase mixture. *J. Anim. Physiol. Anim. Nutr.* **108**, 1624 (2024).
18. Parsi, A., Molet-Rodriguez, A., Martín-Belloso, O. & Salvia-Trujillo, L. *β*-carotene nanoemulsions co-ingested with oatmeal of different viscosities: a semi-dynamic in vitro digestion approach. *Food Res. Int.* **220**, 117143 (2025).
19. Moxon, T., Gouseti, O. & Bakalis, S. In silico modelling of mass transfer & absorption in the human gut. *J. Food Eng.* **176**, 110–120 (2016). Virtualization of Processes in Food Engineering.
20. Marciani, L. et al. Effect of meal viscosity and nutrients on satiety, intragastric dilution, and emptying assessed by MRI. *Am. J. Physiol.* **280**, G1227–G1233 (2001).
21. Wijethunga, A. M., He, Q. S., Prithiviraj, B. & Sun, X. Impact of pretreatments on the techno-functional properties and in vitro digestibility of palmaria palmata proteins. *Food Hydrocoll.* **164**, 111226 (2025).
22. Souto-Prieto, A. et al. Insights into the structuring ability of two brown seaweeds (*Laminaria digitata* and *Saccharina latissima*) for applications as natural texturisers. *Algal Res.* **80**, 103548 (2024).
23. Malafronte, L. et al. Macroalgae suspensions prepared by physical treatments: effect of polysaccharide composition and microstructure on the rheological properties. *Food Hydrocoll.* **120**, 106989 (2021).
24. Ren, X., Sanjeewa, K. K. A., Wang, L. & Mao, X. Fermentation as a strategy to improve the health-promoting benefits of edible seaweeds. *Food Bioprocess. Technol.* **18**, 7827 (2025).
25. Yang, Y., Lin, H. & Fu, X. Fermentation of Pyropia spp. seaweed: a comprehensive review on processing conditions, biological activities and potential applications in the food industry. *Crit. Rev. Food Sci. Nutr.* **65**, 4964–4979 (2025).
26. Maribu, I., Blikra, M. J., Eilertsen, K.-E. & Elvevold, K. Ultrasound and enzymatic processing of palmaria palmata—effects on biochemical components. *LWT* **224**, 117859 (2025).
27. Jacobsen, M. et al. Nutritional and toxicological characteristics of *Saccharina latissima*, *Ulva fenestrata*, *Ulva intestinalis*, and *Ulva rigida*: a review. *Int. J. Food Prop.* **26**, 2349–2378 (2023).
28. Domozych, D. S. et al. The cell walls of green algae: a journey through evolution and diversity. *Front. Plant Sci.* **3**, 82 (2012).
29. El-Sheekh, M. M., Yousuf, W. E., Kenawy, E.-R. & Mohamed, T. M. Biosynthesis of cellulose from *Ulva lactuca*, manufacture of nanocellulose and its application as antimicrobial polymer. *Sci. Rep.* **13**, 10188 (2023).
30. Niklas, W. et al. Cellulose from the green macroalgae *Ulva lactuca*: isolation, characterization, optotracing, and production of cellulose nanofibrils. *Cellulose* **27**, 3707–3725 (2020).
31. Kennedy, C. J., Sturcova, A., Jarvis, M. C. & Wess, T. J. Hydration effects on spacing of primary-wall cellulose microfibrils:: a small angle x-ray scattering study. *Cellulose* **14**, 401–408 (2007).
32. Lopez-Sanchez, P. et al. Nanostructure and poroviscoelasticity in cell wall materials from onion, carrot and apple: roles of pectin. *Food Hydrocoll.* **98**, 105253 (2020).
33. Martinez-Sanz, M., Lopez-Sanchez, P., Gidley, M. J. & Gilbert, E. P. Evidence for differential interaction mechanism of plant cell wall matrix polysaccharides in hierarchically-structured bacterial cellulose. *Cellulose* **22**, 1541–1563 (2015).
34. Lahaye, M., Jegou, D. & Buleon, A. Chemical characteristics of insoluble glucans from the cell-wall of the marine green-alga *Ulva-lactuca* (l) thuret. *Carbohydr. Res.* **262**, 115–125 (1994).
35. Kraithong, S. et al. Potentials of ulva spp.-derived sulfated polysaccharides as gelling agents with promising therapeutic effects. *Int. J. Biol. Nacromol.* **273**, 132882 (2024).
36. Fontes-Candia, C., Diaz-Pinero, L., Vega-Gomez, L. M., Molina-Gilarranz, I. & Martinez-Sanz, M. Relevance of protein-polysaccharide interactions on nutritional quality and gastrointestinal digestion of protein-based foods. *J. Agric. Food Chem.* **73**, 4998–5004 (2025).
37. Marciani, L. et al. Alginate and hm-pectin in sports-drink give rise to intra-gastric gelation in vivo. *Food Funct.* **10**, 7892–7899 (2019).
38. Martínez-Sanz, M., Gidley, M. J. & Gilbert, E. P. Application of X-ray and neutron small angle scattering techniques to study the hierarchical structure of plant cell walls: a review. *Carbohydr. Polym.* **125**, 120–134 (2015).
39. Gunness, P. & Gidley, M. J. Mechanisms underlying the cholesterol-lowering properties of soluble dietary fibre polysaccharides. *Food Funct.* **1**, 149–155 (2010).
40. Diaz-Pinero, L., Fontes-Candia, C., Rodriguez-Dobreva, E., Recio, I. & Martinez-Sanz, M. Influence of bile salts on the gastrointestinal digestion of agar-casein hybrid systems and the nanoassembly of their digestion products. *Food Res. Int.* **197**, 115179 (2024).
41. Yaich, H. et al. Effect of extraction procedures on structural, thermal and antioxidant properties of ulvan from *Ulva lactuca* collected in Monastir coast. *Int. J. Biol. Macromol.* **105**, 1430–1439 (2017).
42. Podolean, I. et al. Catalytic transformation of the marine polysaccharide ulvan into rare sugars, tartaric and succinic acids. *Catal. Today* **383**, 345–357 (2022).
43. Robic, A., Sassi, J.-F., Dion, P., Lerat, Y. & Lahaye, M. Seasonal variability of physicochemical and rheological properties of ulvan in two Ulva species (chlorophyta) from the Brittany coast. *J. Phycol.* **45**, 962–973 (2009).
44. Yaich, H. et al. Effect of extraction conditions on the yield and purity of ulvan extracted from *Ulva lactuca*. *Food Hydrocoll.* **31**, 375–382 (2013).
45. Robic, A., Sassi, J. F. & Lahaye, M. Impact of stabilization treatments of the green seaweed *Ulva rotundata* (chlorophyta) on the extraction yield, the physico-chemical and rheological properties of ulvan. *Carbohydr. Polym.* **74**, 344–352 (2008).
46. Adams, S., Frith, W. J. & Stokes, J. R. Influence of particle modulus on the rheological properties of agar microgel suspensions. *J. Rheol.* **48**, 1195–1213 (2004).
47. Evans, I. D. & Lips, A. Concentration dependence of the linear elastic behaviour of model microgel dispersions. *J. Chem. Soc., Faraday Trans.* **86**, 3413–3417 (1990).
48. Lopez-Sanchez, P. & Farr, R. Power laws in the elasticity and yielding of plant particle suspensions. *Food Biophys.* **7**, 15 (2011).
49. Boehm, M. W., Warren, F. J., Baier, S. K., Gidley, M. J. & Stokes, J. R. A method for developing structure-rheology relationships in comminuted plant-based food and non-ideal soft particle suspensions. *Food Hydrocoll.* **96**, 475–480 (2019).
50. Kidgell, J. T., Magnusson, M., de Nys, R. & Glasson, C. R. Ulvan: a systematic review of extraction, composition and function. *Algal Res.* **39**, 101422 (2019).
51. Jin, Y. et al. An evolving view on food viscosity regulating gastric emptying. *Crit. Rev. Food Sci. Nutr.* **63**, 5783–5799 (2023).
52. Fontes-Candia, C. et al. Nanostructural changes in polysaccharide-casein gel-like structures upon in vitro gastrointestinal digestion. *Food Res. Int.* **169**, 112862 (2023).
53. López-Santamarina, A. et al. Effects of a green seaweed from the Atlantic coast (*Ulva lactuca*) on gut microbiota, using an in vitro colon model. *Food Biosci.* **63**, 105596 (2025).
54. Lopez-Santamarina, A. et al. Potential prebiotic effect of two Atlantic whole brown seaweeds, *Saccharina japonica* and *Undaria pinnatifida*, using in vitro simulation of distal colonic fermentation. *Front. Nutr.* **ume 10**, 1170392 (2023).
55. Brodkorb, A. et al. Infogest static in vitro simulation of gastrointestinal food digestion. *Nat. Protoc.* **14**, 991–1014 (2019).
56. Minekus, M. et al. A standardised static in vitro digestion method suitable for food—an international consensus. *Food Funct.* **5**, 1113–1124 (2014).

57. Pimentel, F. B. et al. Effect of in vitro simulated gastrointestinal digestion on the antioxidant activity of the red seaweed *Porphyra dioica*. *Food Res. Int.* **136**, 109309 (2020).
58. Corona, G. et al. Effect of simulated gastrointestinal digestion and fermentation on polyphenolic content and bioactivity of brown seaweed phlorotannin-rich extracts. *Mol. Nutr. Food Res.* **61**, 1700223 (2017).
59. Kjeldahl, J. Neue methode zur bestimmung des stickstoffs in organischen körpern. *Z. Anal. Chem.* **22**, 366–382 (1883).
60. Barbarino, E. & Lourenço, S. O. An evaluation of methods for extraction and quantification of protein from marine macro- and microalgae. *J. Appl. Phycol.* **17**, 447–460 (2005).
61. Vergara-Patino, L., Sanclemente-Reyes, O. E. & Ararat-Orozco, M. C. Biofixation of CO2 by two species of microalgae grown in photobioreactors. *Acta Biol. Colombiana* **28**, 5–11 (2023).
62. Leyton, A. et al. Identification and efficient extraction method of phlorotannins from the brown seaweed *Macrocystis pyrifera* using an orthogonal experimental design. *Algal Res.* **16**, 201–208 (2016).
63. Lopez-Sanchez, P. et al. Effect of mechanical and thermal treatments on the microstructure and rheological properties of carrot, broccoli and tomato dispersions. *J. Sci. Food Agric.* **91**, 207–217 (2011).
64. CELLS,. Alba synchrotron. https://www.albasynchrotron.es/es (2023).
65. Kieffer, J. & Wright, J. P. Pyfai: a Python library for high performance azimuthal integration on GPU. *Powder Diffr.* **28**, S339–S350 (2013).
66. Ilavsky, J. & Jemian, P. R. Irena: tool suite for modeling and analysis of small-angle scattering. *J. Appl. Crystallogr.* **42**, 347–353 (2009).
67. RCoreTeam. A language and environment for statistical computing (2023).

Acknowledgements

The authors would like to thank Lucía Sánchez and Laura Gómez from the Institute of Marine Research (IIM-SIC) for assistance with confocal scanning laser microscopy. Jakob Ytterberg and Anna Ström are gratefully acknowledged for performing ζ potential measurements.

Author contributions

A.S.P., A.C., M.M.S. and P.L.S. wrote the original draft. T.F., Z.C., L.D. and M.M.S. conducted formal analysis and investigation. A.S.P., Z.C., L.D. and M.M.S. contributed to experimental design and data analysis. P.L.S. conceptualised and designed the methodology of this study. All authors reviewed and edited the paper.

Competing interests

The authors declare no competing interests.

Additional information

Supplementary information The online version contains supplementary material available at https://doi.org/10.1038/s41538-025-00639-w.

Correspondence and requests for materials should be addressed to Antonio Souto-Prieto or Patricia Lopez-Sanchez.